IEEE Access
Multidisciplinary | Rapid Review | Open Access Journal

SPECIAL SECTION ON ADVANCED OPTICAL IMAGING FOR EXTREME ENVIRONMENTS

Received May 31, 2019, accepted June 20, 2019, date of publication July 3, 2019, date of current version July 25, 2019.

Digital Object Identifier 10.1109/ACCESS.2019.2926653

Adaptive Wavelet Filter With Edge Compensation for Remote Sensing Image Denoising

BOYANG CHEN[1], XUAN FENG[2], RONGHUA WU[1], QIANG GUO[1], XI WANG[1], AND SHIMING GE[3], (Senior Member, IEEE)

[1]National Satellite Meteorological Center, Beijing 100081, China
[2]Institute of Information Engineering, Chinese Academy of Sciences, Beijing 100095, China
[3]Technology and Engineering Center for Space Utilization, Chinese Academy of Sciences, Beijing 100094, China

Corresponding author: Shiming Ge (geshiming@iie.ac.cn)

This study was supported by National Natural Science Foundation of China (41375023 and 61772513), National Key Research and Development Plan (2016YFC0801005), the Open Foundation Project of Robot Technology Used for Special Environment Key Laboratory of Sichuan Province in China (Grant No. 16kftk01). The work of S. Ge was also supported by the Open Projects Program of National Laboratory of Pattern Recognition, Ant Financial through the Ant Financial Science Funds for Security Research, and the Youth Innovation Promotion Association, Chinese Academy of Sciences.

ABSTRACT Advanced Geostationary Radiation Imager (AGRI) is one of the main payloads of the second-generation geostationary orbit meteorological satellite, FengYun-4A. Typically, the existence of variable stripe noise in the water vapor band remote sensing images of the AGRI greatly affects many applications, such as cloud detection, especially as one full disk image is separated into ten sub-images for transforming as soon as possible, so the denoising algorithm, which can reduce variable stripe noise and is adaptive to process using sub-images, must be built. In this paper, we propose an adaptive wavelet filter for image denoising. This approach introduces a new parameter termed weight sum variance of digital number probability (WSVODP), which is used to indicate the appropriate wavelet filter coefficients. WSVODP is only sensitive to the difference of observation targets of different sensors. Thus, our approach can learn appropriate wavelet filter coefficients fast and exactly. We built a real-world remote sensing image dataset from AGRI on FengYun-4A, and the experimental results on this dataset show that the proposed approach could effectively reduce the variable stripe noise from different observation targets. At the same time, an edge compensation method, which is fitted to the scanning model of the AGRI, is suggested to avoid ringing artifacts. Many applications, such as cloud detection with denoised images, show very good results. The proposed approach reduces the stripe noise adaptation, so the result is very steady even if the stripe noise varies with different targets, and edge compensation ensures that there are no obvious ringing artifacts in the full disk image joined by the ten sub-images.

INDEX TERMS Geostationary meteorological satellite, water vapor, stripe noise, non-uniformity, wavelet filter, image measurement, denoising.

I. INTRODUCTION

The FengYun-4 (FY-4) geostationary meteorological satellite is a 2nd generation geostationary meteorological Chinese satellite. The first FY-4 satellite named FY-4A was launched successfully on Dec. 11 2016. An Advanced Geostationary Radiation Imager (AGRI) is one of the main payloads on FY-4A, as shown in table1, whose characters are very similar as that of the apparatus of other countries. It is very important for observing the area from E40° to E160°. There are 4 sensors for every infrared channel. It is found that obvious stripe noise exists in the water vapor (6.9μm-7.3μm) image of AGRI. The stripe noise leads to very poor performance such as in cloud detection. A Comb-type cloud appears and this is obviously impossible. Therefore, a useful algorithm to reduce stripe noise is needed, or all the predictions based on water vapor images appear with Comb-type errors.

The characters of different sensors in one linear array detector are always different. The stripe noise is a common noise in remote sensing images from the visible band to micro wave band [1]–[5]. Many analyses and denoising methods are proposed. However, the reason for traditional stripe noise is usually the response non-uniformity of the different sensors. However, the reason for stripe noise in an AGRI is different from that of traditional stripe noise. The difference of spectral response function (SRF) of different sensors leads to the stripe noise. In the water vapor band, the absorption peak in water vapor band amplifies the difference of SRF of sensors,

The associate editor coordinating the review of this manuscript and approving it for publication was Huimin Lu.

TABLE 1. Geostationary meteorological satellite imagers.

Imager	Vis	Near Infrared	Infrared	Temporal	SNR (Vis)	NEDT (Infrared)	MTF	Location
VISSR	1.25km	—-	5km	30min	—-	—-	—-	E99.5°
AGRI	0.5-1km	2km	4km	15min	SNR=200@ρ=100%	NEDT=0.2k@300k	>0.2	E105°
ABI	0.5-1km	1km	2km	5min	SNR=200@ρ=100%	NEDT=0.2k@300k	>0.2	W77°
FCI	0.5-1km	1km	2km	10min	SNR=300@ρ=100%	NEDT=0.1k@300k	>0.2	E0°

so the serious stripe noise appears in water vapor images of AGRI, and stripe noise caused by different SRF is different from the stripe noise caused by response non-uniformity and it is variable stripe noise. Traditional algorithms are good at reducing the noise caused by response non-uniformity, but they not good at denoising the AGRI water vapor image with variable stripe noise.

In the past decades, researchers paid attention on how to reduce the stripe noise of remote sensing images, and all the algorithms are classified calibration-based and scene-based. Scene-based algorithms mainly include algorithms that are statistics-based, neural network-based, variation model-based, and filter-based algorithms. Calibration algorithms [6], [7] have been widely used in correcting the non-uniformity for remote sensing images, however, calibration algorithms need calibration hardware and many remote sensing apparatus does not have calibration hardware, and the response of infrared sensors always changes after time. The calibration coefficients do not fit the images taken after a long time.

In order to reduce the variable stripe noise caused by different SRF, this paper proposes a learning adaptive wavelet filter (LAWF). The algorithm uses a new measurement parameter termed Weight Sum Variance of Digital Number Probability (WSVODP) to determine the appropriate adaptive filter coefficients. The results demonstrate that the stripe noise in water vapors image is very clearly reduced.

This work focuses on the variable stripe noise. The contribution in this field can be expressed as follows:

- [1] To study the algorithm for variable stripe noise, we built a dataset using more than one year's remote sensing images in the water vapor band.
- [2] Propose a new learning adaptive wavelet filter based on a new measurement parameter termed WSVODP. This parameter indicates the appropriate filter coefficients for each image, and a good denoising result appears for every image. Specifically, WSVODP does not need the characteristics of the stripe noise as the filter coefficients can be confirmed fast and exactly.
- [3] The new algorithm is used to reduce the stripe noise of the water vapor images of AGRI on FY-4A. These denoising images without stripe noise are used well for many applications such as cloud detection.

II. RELATED WORK

Many methods for reducing stripe noise have been researched. The article [8] introduces a restraining stripe noise algorithm based on a local histogram specification. This algorithm uses a harmonic mean histogram as the goal of adjusting the histogram and corrects infrared images. This histogram specification algorithm demands that the responses of the sensors are stable during all observations.

In recent years, algorithms based on variation models have made significant progress. In article [9], Shen and Zhang first proposed the Huber-Markov variation model to reduce the stripe noise. Recently, Lu *et al.* [10] and Zhang *et al.* [11] introduced low rank prior-based destriping methods. In article [12] an algorithm based on total variation model is used to reduce the stripe noise of MODIS and hyperspectral images. Although the variation-based methods have achieved encouraging destriping performance [13], they still face some problems. These are that most of them focus on properties of the image, few of them take into account the characteristic of the stripe noise, hence, many image details may be removed along with the destriping.

Neural network algorithms are used to reduce stripe noise of remote sensing images. D. A. Scribner uses a BP neural network to denoise infrared images first [14]. Many methods based on BP neural network have been proposed. The articles [15] to [17] improve BP neural network algorithms. Not only BP neural networks have been used but also deep convolutional neural networks are also used for destriping [18]. However, whatever the network is, they need many samples to train the network coefficients [19]. That means non-uniformity must be stable, or the coefficients are not suitable.

Another kind of algorithm is filter-based and a wavelet filter is one of the main filter models. A wavelet coefficients threshold denoising method is proposed by Donoho [20], and many other users have widely used it because of its simple principle [21] to [23]. The article [24] introduces an algorithm based on media filter and wavelet transform, a set of processes based on wavelet transform are introduced in article [25], but the main goal is not stripe noise. An algorithm for wide-stripe noise is introduced in article [26]. Article [27] proposes an algorithm by wavelet moment matching and it assumes that the stripe noise is caused by the different gain and offset of the sensors. In addition, a steering kernel algorithm [28], guided filter algorithm [29], [30] and bilateral filter algorithm [31] and so on [32] are all suggested. All have advantages and disadvantages.

All the conclusions provide a basis for the research on learning adaptive wavelet filter for remote sensing image denoising. In work it is found that, most algorithms need the stable response of the sensors in order to use constant correction coefficients, few of them take into account variable

stripe noises, and although some algorithms mentions adaptive, the characters of stripe noise must be known. But it is impossible to some images with seriously variable stripe noises.

III. ANALYSIS ON STRIPE NOISES OF AGRI

A. OVERVIEW OF AGRI

As shown in figure1, there are 4 sensors for every infrared channel of AGRI. The scanning direction is along east-west and a full disk image needs 687 mechanical-scanning lines, so the data in one line is collected by the same sensor, as shown in figure2. It is found that the direction of stripe noise is along east-west too. We are sure that the stripe noise is from different sensors.

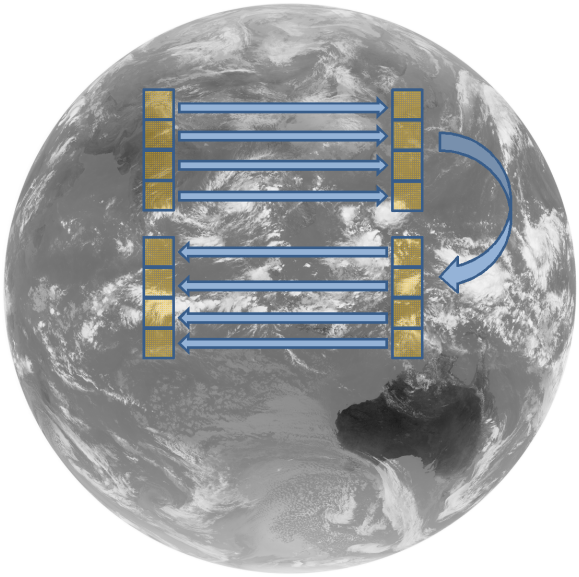

FIGURE 1. The sensors and scanning direction.

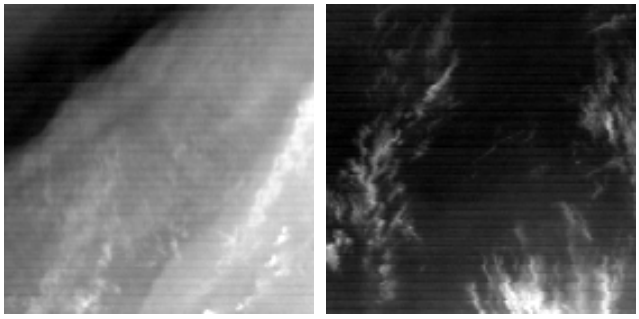

(a) (b)

FIGURE 2. Water vapor band images of AGRI (a) The cloud image (b) The earth surface image.

Figure2 is picked from a random sequence of images. The stripe noise is very clear. However, after analyzing the image carefully, there are some interesting details the appearance of which is not mentioned in any other article. Firstly, the stripe noise of the water vapor image is not a constant brighter or darker line. The stripe noise value may be brighter or darker even in one line and the noise is not linked to any sensor. Secondly, the noise value varies with the variation of physical targets. Analyzing the appearance of stripe noise, they fact that noise is not constant with any sensor demonstrates that stripe noise is not caused by the response non-uniformity, and the variations in brightness difference shows that the difference caused in stripe noise is caused by physical targets. Therefore, it is reasonable to conclude that the stripe noise of AGRI is not stable. Besides, comparing the nearest two lines in a smooth area, it is found that the brightness temperature gradient of the near two pixels along north to south can reach 1k. Because most productions based images use brightness temperature to classify the physical targets, so a wrong gradient of brightness temperature leads to inaccurate results.

B. ANALYZE ABOUT STRIPE NOISE

Stripe noise appears only in water vapor band images. The variation of stripe noise makes us focus on the SRF, the atmosphere transmissivity. The SRF of water vapor band and far infrared band are shown in figure3a while the zoom in area of water vapor band SRF is shown in figure3b and the zoom in area of far infrared band SRF is shown in figure3c. In the figure we can see that many absorption peaks exist in the water vapor band and the different SRF of 4 sensors leads to different physical targets though the sensors observe the same area. A small difference of SRF makes a big difference to the brightness temperature in the water vapor band and when the sensors observe the different targets, the stripe noise value always varies with the variation of targets.

Based on the water vapor images, it is certain that the stripe noise of AGRI is variable stripe noise. This is very different from that of traditional remote sensing images. The image noise is usually defined from the mathematical point of view in that the image can be regarded as a spatial function, and the noise can be regarded as additive noise. The relation can be expressed by the following formulas:

$$f_n = f + n \tag{1}$$

where f_n represents the image collected.

The radiance received by two sensors $a1$ and $a2$, are formula 2 and 3.

$$R_{a1} = \sum R_{(\lambda)} * \psi 1_{(\lambda)} \tag{2}$$

$$R_{a2} = \sum R_{(\lambda)} * \psi 2_{(\lambda)} \tag{3}$$

where $R_(\lambda)$ is the radiance from the target, and $\psi_(\lambda)$ is the SRF of the sensor.

For the stripe noise caused by SRF, it is very difficult to confirm whose SRF is right or wrong and this means the stripe noise is only from the different targets observed by different sensors. Here assume the sensor $a1$ is the standard sensor. So

$$R_{a2} = R_{a1} + R_n = R_{a1} + R_{a2} - R_{a1} \tag{4}$$

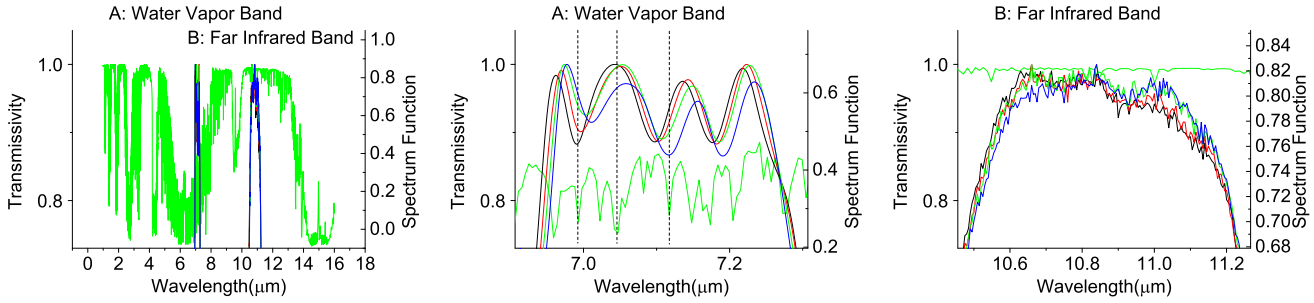

FIGURE 3. The atmosphere transmissivity and SRF of AGRI (a) Atmosphere and SRF of AGRI (b) Zoom in area of water band SRF, where many absorb peaks (c) Zoom in area of far infrared band, where the atmosphere transmissivity is very smooth.

Compare with formula 1, then

$$\begin{aligned} R_n &= R_{a2} - R_{a1} \\ &= \sum R_{(\lambda)} * \psi 2_{(\lambda)} - \sum R_{(\lambda)} * \psi 1_{(\lambda)} \\ &= \sum R_{(\lambda)} * (\psi 2_{(\lambda)} - \psi 1_{(\lambda)}) \end{aligned} \tag{5}$$

From the formula5, obviously, the noise $\sum R_{(\lambda)} * (\psi 2_{(\lambda)} - \psi 1_{(\lambda)})$ not only has a relationship with the radiance of the observing targets, but also has a relationship with the SRF of the sensor. Radiance and SRF is convolution. Comparing with the stripe noise caused by response non-uniformity, which is described in formula6, while the SRF of different sensors are the same, the noise is only the linear amplification of the radiance of the observing targets by response coefficients k of the sensors. It is easy to reduce this kind of stripe noise by adjusting the response coefficients and this is the aim of most traditional algorithms, such as histograms specification algorithm and BP neural network algorithm and so on. However, convolution between radiance of the target and the SRF of the sensor means the stripe noises cannot be described by a linear function, so it cannot be reduced by adjusting constant response coefficients, so traditional algorithms used for stripe noises caused by response non-uniformity are not good at reducing variable stripe noise. A new denoising method used for variable stripe noises must be built.

$$R_{nk} = R * (k_2 - k_1) \tag{6}$$

C. MEASUREMENTS OF IMAGE DENOISING

Many typical parameters are used for measurements of image denoising, such as the peak of signal to noise (PSNR), which is shown in formula7.

$$PSNR = 10 * \lg \frac{DN_{\max}^2}{\frac{1}{M*N} \sum_{x=1}^{M} \sum_{y=1}^{N} [f'(x,y) - f(x,y)]^2} \tag{7}$$

where $f(x, y)$ is the standard image, that is the image without any nose, and $f'(x, y)$ is the processed image, $M * N$ is the size of the image.

Normalized mean square error (NMSE) is another measurement parameter, which is shown in formula8.

$$NMSE = \frac{\sum_{x=1}^{M} \sum_{y=1}^{N} [f'(x,y) - f(x,y)]^2}{\sum_{x=1}^{M} \sum_{y=1}^{N} f(x,y)^2} \tag{8}$$

where $f(x, y)$ is the standard image, and $f'(x, y)$ is the processed image, $M * N$ is the size of the image.

The average gradient value of the image (AGVI) is also an measurement parameter, which is shown in formula9.

$$AGVI = \frac{1}{M*N} \sum_{x=1}^{M} \sum_{y=1}^{N} [(\nabla x.f(x,y))^2 - (\nabla y.f(x,y))^2]^{1/2} \tag{9}$$

where $\nabla x.$ and $\nabla y.$ are the gradient operator of the direction x and direction y, $M * N$ is the size of the image.

However, after analyzing all the measurement parameters, it is found that some parameters like PSNR and NMSE using the original images are not suitable for real remote sensing images, and some parameters like AGVI do not include any direction information. To measure the denoising image exactly, two new measurement parameters are suggested. One parameter is named the harshness information with separated direction (HISD), and HISD is a set of parameters, which is shown in formula10. It demonstrates details of the image that are very different from all the parameters mentioned above.

$$\begin{aligned} HISD_{-x} &= \{\frac{1}{N} \sum_{y=1}^{N} [\nabla x.f'(x,y)]^2\}^{1/2} \\ HISD_{-y} &= \{\frac{1}{M} \sum_{x=1}^{M} [\nabla y.f'(x,y)]^2\}^{1/2} \\ HISD_{-p} &= \frac{[HISD_{-y}(f'') - HISD_{-y}(f')]/HISD_{-y}(f'')}{[HISD_{-x}(f'') - HISD_{-x}(f')]/HISD_{-x}(f'')} \end{aligned} \tag{10}$$

where f'' is the observing image, it is not the standard image, so HISD is very suitable to measure the real observed images.

$HISD_{-x}$ is the measurement of direction x, it demonstrates the harshness of direction x, $HISD_{-y}$ is the measurement of direction y, it demonstrates the harshness of direction y, $HISD_{-x}$ and $HISD_{-y}$ directly demonstrate how serious the stripe noises are. Especially, $HISD_{-p}$ is the phase of the denoising algorithm. It demonstrates that the denoising process is along a particular direction, so the HISD demonstrates whether the algorithm is along the direction of the stripe noise or not.

Another new measurement parameter is WSVODP, which is shown in formula13. The advantage of this is that it does not need the edge information of the image while being measured, so it is not influenced by the gradient value of the images, it is only sensitive to stripe noise.

$$P_i = S_i / \sum_{i=0}^{Q-1} S_i \tag{11}$$

$$VODP_{(i)} = (E\{(P_{i,k} - E(P_{i,k})^2)\})^{1/2}, i \in [0, Q-1] \tag{12}$$

$$WSVODP = \sum_{i=0}^{Q-1} VODP_{(i)} * \sum_{j=1}^{DetN} Num_{(i,j)} \tag{13}$$

The WSVODP parameter is calculated by formula11 to 13. Firstly, the Digital Number Probability is calculated by formula11, where S_i is the number of pixels whose DN is i, the whole DN range is [0,$Q-1$]. Secondly, VODP is calculated by formula12, where the VODP demonstrates the difference of the response of all the sensors to a specific target, and the VODP curve shows the response of all the sensors in the whole DN range. Lastly, WSVODP is calculated by the formula13. $Num(i,j)$ is the quantity of pixels whose digital number is i in observing data of sensor j and it is calculated by the pixel number of observed data, so it does not need the edge information of the image but is only sensitive to stripe noise.

IV. PROPOSED ALGORITHM

A learning adaptive wavelet filter (LAWF) based on WSVODP parameter is proposed to reduce the stripe noise of AGRI. As the stripe noise of AGRI is along east-west in the images and it is typical horizontal stripe noise, the algorithm uses a wavelet filter to separate horizontal information and the filter coefficients are determined adaptively by the WSVODP parameter.

A. THE BASIC PRINCIPLE OF IMAGE DENOISING BASED ON WAVELET TRANSFORM

The wavelet transform is a time-frequency analysis method of signal processing. It is suitable for non-linear and non-stationary signal processing, at the same time, it is a multi-scale and multi-directional processing method. Three high-frequency sub-images and a low-frequency sub-image can be obtained after an image is decomposed by wavelet transform; three high-frequency sub-images contain the information of horizontal, vertical, and diagonal directions, respectively. The 4 sub-images are named $LL_$image, $LH_$image, $HL_$image, and $HH_$image, and the sub-images show the image information at a different frequency compared with the original image. The wavelet filter adjusts the sub-image information and, at the last stage restores the image using the adjusted sub-images. Here, the sub-image means that the image is obtained after decomposing an image with wavelet transform, and one ′sub-image′ can also be decomposed with wavelet transform, so the wavelet filter is not the only layer, but can be many layers.

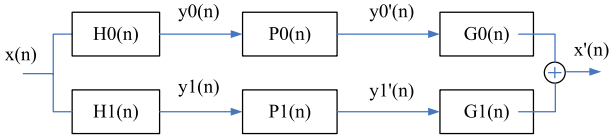

FIGURE 4. Process of wavelet filter.

The whole wavelet filter process is in figure4. A signal $x(n)$ is decomposed by wavelet transform, and sub-image information is adjusted by processing, which after that reconstruction will generate a new signal $x'(n)$. From the process we can see that, the key to image denoising based on wavelet filter is adjustment of wavelet coefficients determined by the wavelet filter parameters.

B. RESEARCH ON WAVELET FILTER

The idea of image denoising based on wavelet transform can be divided into two kinds. One is that the image signal and noise signal show different laws in different resolutions after wavelet transform. The wavelet coefficients are adjusted to achieve denoising. The other is to combine wavelet transform with a traditional image denoising algorithm to improve the performance of the original image denoising algorithm by utilizing the characteristics of wavelet transform multi-resolution and time-frequency localization. The analysis above demonstrates that stripe noise is a kind of high-frequency noise, and it is variable in different images, so an adaptive denoising algorithm is absolutely necessary.

$$\begin{bmatrix} cY1 * LL & cY2 * LH \\ cY3 * HL & cY4 * HH \end{bmatrix}_Y \tag{14}$$

A wavelet filter may be written as formula14, which is the key process unit in figure4, Where Y is the wavelet transform layer number, the wavelet transforms with different layer decomposition in the image at different frequencies. Because the stripe noise in water vapor images of AGRI is along the horizontal direction, the coefficients can be set from formul 15 and 16.

$$cK1 = cK3 = cK4 = 1 \quad K \in [1, Y] \tag{15}$$

$$cY2 = st \quad st \in [0, 1) when K = Y$$

$$cK2 = 0 \quad K \in [1, Y-1] \tag{16}$$

Formul15 and 16 ensure that only the horizontal information is reduced. Wavelet transform layer Y and restraining coefficient st are very important to the denoising result.

They are determined by WSVODP parameter in proposed algorithm.

C. ADAPTIVE WAVELET FILTER FOR DENOISING

The advantage of learning adaptive wavelet filter is to confirm the most appropriate wavelet filter coefficients using the proposed measurement parameter WSVODP. The details of the method is in Algorithm1, and the appropriate wavelet filter coefficients are determined by WSVODP parameter in formula17.

$$\begin{aligned} \nabla WP_i &= WSVODP_i - WSVODP_{i+1} \quad i \in [1, LN-1] \\ iC &= \min\{i | \nabla WP_i < \varepsilon \quad i \in [1, LN-1]\} \end{aligned} \tag{17}$$

where LN is the number of wavelet transform, ε is the smoothing threshold. The general steps of learning for the adaptive wavelet filter for denoising are as follows:

1) [1] Decomposing the input image by wavelet filtering. The transformation layer is set to $LayTmax$. This is the process from line1 to line4 in the algorithm pseudo-code.
2) [2] Set $delt = 0.1$. This is the step distance of restraining coefficient of the filter and is the process is line5 in the algorithm pseudo-code.
3) [3] For each image, the most appropriate coefficients are found in $(LayTmax - 1)/delt$ sets of potential filter coefficients, so the circular variable j is from 1 to $(LayTmax - 1)/delt$ and is line6 in algorithm pseudo-code.
4) [4] Calculate $LayT$ and st, $LayT$ is the current layer number of the filter where st is the restraining coefficient and this process is from line7 to line9 in algorithm pseudo-code.
5) [5] Filter the input image using the current coefficients $LayT$ and st in line10.
6) [6] Compose the image using Sub_images after filtering in the process from line11 to line13.
7) [7] Measure the image using the WSVODP parameter and restore the filter parameters $LaytT$, st from line14 to line20.
8) [8] Confirm the appropriate filter coefficients adaptation using equation17 in line22.
9) [9] Re-do the filter on the input image using the appropriate coefficients.
10) [10] Output the image after denoising from lines24 to line25.

Of course, for reducing the time for confirming the most appropriate wavelet filter coefficients, two-step work can be done. Firstly, use lots of images to calculate WSVODP in order to learn the basic wavelet filter coefficients. Lots of images ensure that the basic wavelet filter coefficients are near the most appropriate wavelet filter coefficients for each image. Then when near the basic wavelet filter coefficients, a small-step adaptive adjustment to wavelet filter coefficients can be been done for confirming the most appropriate wavelet filter coefficients for every image.

D. EDGE COMPENSATION

The scanning model of AGRI is from north to south with 4 infrared sensors observing 4-lines of data per mechanical-scanning line from west to east and 687 mechanical-scanning lines of data make a full disk image of 2748 × 2748 pixels. A full disk image of AGRI is separated into 10 sub-images for transforming as soon as possible. This means an image with 2748 × 2748 pixels is separated into 9 sub-images of 280 × 2748 pixels and 1 sub-image of 228 × 2748 pixels. The wavelet filter process starts just after sub-image data collection finishes. The denoising is performed on every sub-image. However, obvious gray value bias appears at the joint of 2 sub-images as shown in figure5a. The data in the same column of images before and after the process is plotted in figure6 where the red line is the data from original image and the green line is the data from processed image. They are almost the same and that demonstrates the wavelet filter only reduces stripe noise. A big departure of two lines occurs at the bottom of every sub-image and this is caused by a bad edge to the image.

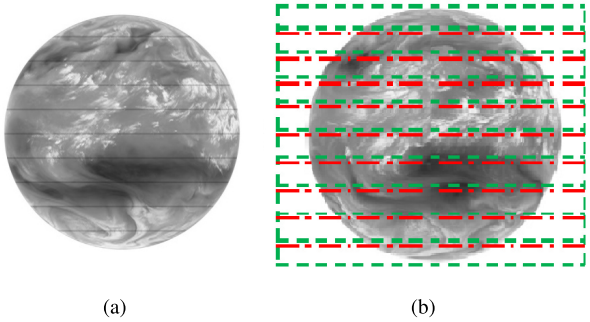

FIGURE 5. The images (a) Without edge compensation (b) With edge compensation.

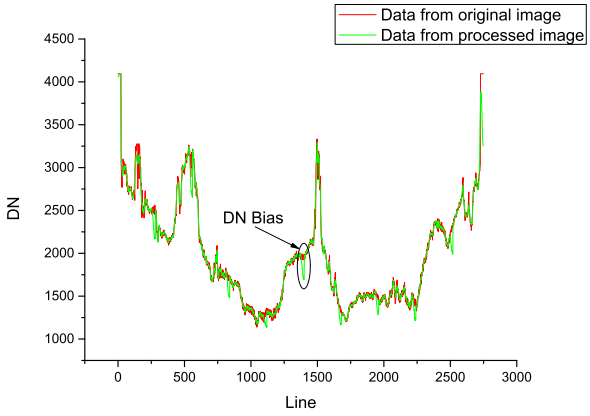

FIGURE 6. Data in the same column of original images and image processed.

An image can be generated by wavelet transform coefficients via formula 18, and the noise reduced by the wavelet filter can be described as formula 19, obviously, the noise

Algorithm 1 Learning Adaptive Wavelet Filter (LAWF)

Require: The image I to be processed, scale $M \times N$
Ensure: The image I' processed, scale $M \times N$

1: $Sub\_LL = I$
2: **for** $i = 1 \rightarrow LayTmax$ **do**
3: $\begin{bmatrix} Sub\_LL \\ Sub\_LH \\ Sub\_HL \\ Sub\_HH \end{bmatrix}_i = WVF(Sub\_LL_{i-1})$
4: **end for**
5: $delt = 0.1$
6: **for** $j = 1 \rightarrow (LayT\ \max - 1)/delt$ **do**
7: $stA = 1 + (j-1) * delt$
8: $LayT = floor(stA)$
9: $st = stA - LayT$
10: $Sub\_LH'_i = \begin{cases} 0 & i < LayT \\ st \times Sub\_LH_i & i = LayT \\ Sub\_LH_i & i > LayT \end{cases} \quad i \in [1, LayT\ \max]$
11: **for** $i = LayTmax \rightarrow 2$ **do**
12: $Sub\_LL_{i-1} = WVF^{-1}\left(\begin{bmatrix} Sub\_LL \\ Sub\_LH' \\ Sub\_HL \\ Sub\_HH \end{bmatrix}_i\right)$
13: **end for**
14: $I' = Sub\_LL_1$
15: $S_i^{(1,2,\cdots,DetN)} \leftarrow$ The number of pixels whose DN is i in image I' for sensor $1 \rightarrow DetN$
16: $P_i^{(1,2,\cdots,DetN)} = S_i^{(1,2,\cdots,DetN)} / \sum_{i=0}^{Q-1} S_i^{(1,2,\cdots,DetN)}$
17: $VODP_i = (\frac{1}{DetN} \sum_{j=1}^{DetN} (P_i^j - \frac{1}{DetN} \sum_{k=1}^{DetN} P_i^k)^2)^{1/2}, i \in [0, Q-1]$
18: $WSVODP_j = \sum_{i=0}^{Q-1} \left(VODP_i \times \sum_{j=1}^{DetN} S_i^j \right)$
19: $LT_j = LayT$
20: $ST_j = st$
21: **end for**
22: $\nabla WP_i = WSVODP_i - WSVODP_{i+1}, i \in [1, length\,(1 : delt : LayT\ \max) - 1]$
$iC = \min\{i | \nabla WP_i < \varepsilon, i \in [1, length\,(1 : delt : LayT\ \max) - 1]\}$
23: Do line 10 to 14 using parameters LT_{iC} and ST_{iC}
24: $I' = Sub\_LL_1$
25: Return I'

reduced $\Delta f(x, y)$ is a high-frequency image along horizontal direction.

In the frequency domain, the power of the original image is in formula20 where $w1$ is the cut-off frequency of the optical system observing the image, and also, the power of the image processed can be described by formula21 where $w2$ is the cut-off frequency of the wavelet filter. Of course, $w2 < w1$. A cut-line in the frequency domain causes the departure of two lines in figure, which is a ringing artifact.

$$f(x, y) = \frac{1}{\sqrt{MN}} \sum_m \sum_n W_\varphi(j_0, m, n)\varphi_{j_0,m,n}(x, y) + \frac{1}{\sqrt{MN}} \sum_{i=H,V,D} \sum_{j=j_0}^{\infty} \sum_m \times \sum_n W_\phi^i(j, m, n)\varphi_{j,m,n}^i(x, y) \quad (18)$$

$$\Delta f(x, y) = -\frac{1}{\sqrt{MN}} \sum_{j=j_T}^{\infty} \sum_m \sum_n W_\phi^H(j, m, n)\varphi_{j,m,n}^H(x, y) \quad (19)$$

$$P1 = E\left\{ \left| f_1(t) - \overline{f_1(t)} \right|^2 \right\} = \int_{-w1}^{w1} P(w)dw \quad (20)$$

$$P2 = E\left\{ \left| f_2(t) - \overline{f_2(t)} \right|^2 \right\} = \int_{-w2}^{w2} P(w)dw \quad (21)$$

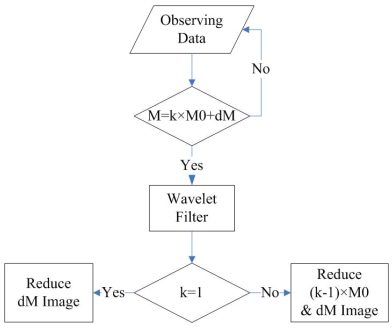

FIGURE 7. The process flow of the edge compensation.

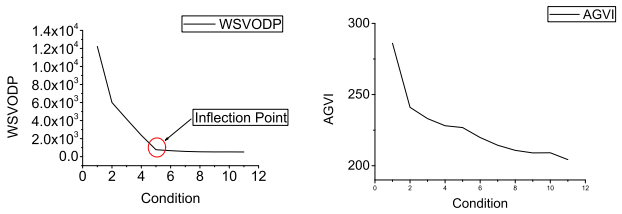

(a) (b)

FIGURE 8. Measurements for different process conditions (a) WSVODP curve (b) AGVI curve.

For avoiding a ringing artifact, based on the scanning model of AGRI of FY-4A, a new process is designed. The process is shown in figure7. The steps are as follows:

- [1] Receive the observing data line by line.
- [2] k is the sequence number of the image to be processed, k, M0 is the line number of one sub-image, and dM is the line number of edge compensation. The process starts when M reaches the threshold designed. In figure 8b, the green-line is the real edge of every sub-image, and the red-line is the compensative edge. dM is the distance between the green-line and red-line.
- [3] The wavelet filter is applied to the whole image received.
- [4] If the sub-image is the first image, the dM image is reduced after the wavelet filter, or both the (k-1)×M0 image and dM image are reduced after the wavelet filter.

Comparing with the figure 5a, a gray value dropping per every 280 lines does not appear in figure 5b, as the edge compensation ensures that the ringing artifact does not occur at the real bottom of the sub-image.

Based on the statisticals information of the images from the AGRI, the area of ringing artifacts is about 30-50 lines, so the line number of edge compensation is set to 100 and, that means dM= 100. The observing time for a full disk is about 15 minutes, which includes black-body observation, star observation and deep space observation, and according to the infrared sensors array, 100 lines data is from 25 mechanical-scanning lines, so the time delay for edge compensation is $\Delta time < \frac{15*60}{687} * \frac{100}{4} \approx 33(s)$, and therefore, a very small time delay.

V. EXPERIMENTS AND DISCUSSION

A. CONFIRMING THE COEFFICIENTS

In this paper, images from Feb. 1 in 2018 to Mar. 3 in 2018 are processed to analyze the filter coefficients using different layer numbers of wavelet transform and different restraining coefficients to denoise the images. The parameters are shown in table2. In table2, with the cut-off frequency of the filter dropping, the AGVI of the image processed becomes smaller and smaller and that means the stripe noise is reduced. However, a low-pass filter could blur the image more or less, but this is unavoidable while reducing stripe noise, and it is very difficult to determine the appropriate filter coefficients by traditional measurement parameters, since they use the edge information from the image.

TABLE 2. Filter coefficients and measurements.

NO.	Y	st	WSVODP	AGVI
1	Original Image	-	1.222×10^4	286.1
2	2	c22=0.6	6.003×10^3	233.1
4	2	c22=0.2	2.375×10^3	228.1
5	2	c22=0	7.718×10^2	226.8
6	3	c32=0.8	6.620×10^2	219.8
7	3	c32=0.6	5.828×10^2	214.4
8	3	c32=0.4	5.418×10^2	210.8
9	3	c32=0.2	5.252×10^2	209
10	3	c32=0	5.280×10^2	209.1
11	4	c42=0.8	5.179×10^2	204.3

The values of WSVODP and AGVI in table2 are shown as curves in figure8. According to figure8, from condition 1 to condition 5, the WSVODP value also drops down quickly and that means a better result in reducing stripe noise. After the 6th condition, the WSVODP curve becomes smooth and the reason is that WSVODP is calculated out by the quantity variance of pixels at the same digital number. The heavier stripe noise is, the bigger WSVODP is. It is only sensitive to the non-uniformity.

The difference between measurement parameters WSVODP and AGVI is very obvious, one inflection point appears in WSVODP curve, and that does not appear in AGVI curve. Condition no.6 is the inflection point of the WSVODP curve, and the coefficients are appropriate filter coefficients. FWSVODP is better than traditional measurement parameters for determining the filter coefficients, ε for water vapor images of AGRI set to 100. Coefficient $c32 = 0.8$ is used as the wavelet filter coefficients.

B. RESULTS

The denoised image of figure2a is shown in figure9 and the denoised image of figure2b is shown in figure10. One image is a typical bright target, and another image is a typical dark target. The images are all selected at random in all the processed images, and the results of all images are similar.

The comparison methods include histogram specification, mean value filter, BP neural network, convolution neural network(CNN) and our method. The Histogram specification algorithm and the BP neural network algorithm are typical

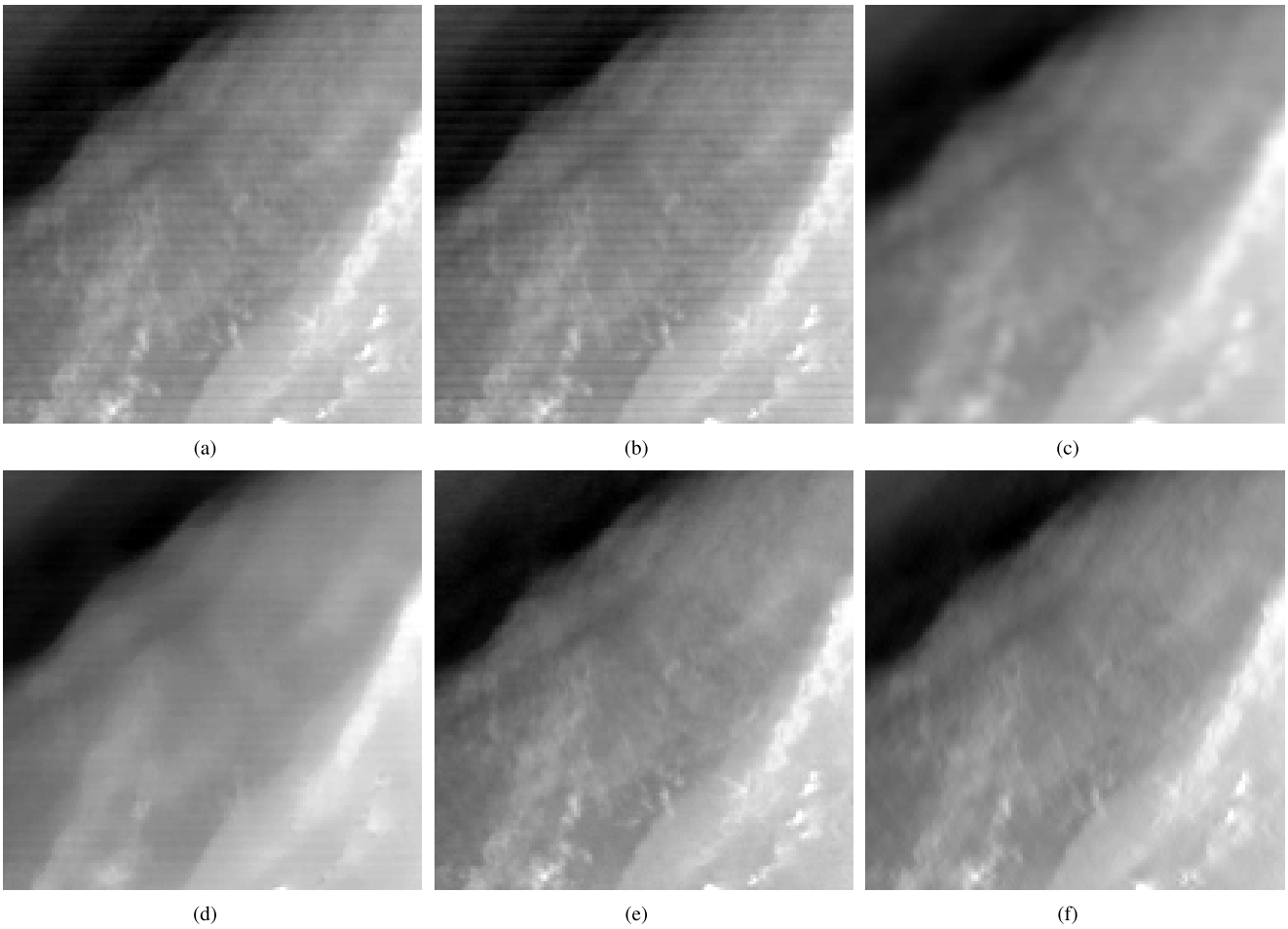

FIGURE 9. Cloud images processed by (a) Original image (b) Histogram adjusting (c) Mean Value filtering (d) BP neural network (e) Convolution neural network (f) Ours.

TABLE 3. The measurements of the denoised images in figure9.

Image		a	b	c	d	e	f
WSVODP		660.559	410.484	214.68	992.714	142.543	69.269
	X	178.598	178.465	102.563	80.988	185.138	174.043
HISD	Y	200.803	248.401	93.939	93.433	142.521	111.984
	P	—	-320.357	1.25	0.978	-7.926	17.344

TABLE 4. The measurements of the denoised images in figure10.

Image		a	b	c	d	e	f
WSVODP		267.235	358.482	88.272	115.749	86.200	89.485
	X	127.935	127.84	92.36	84.788	112.173	124.059
HISD	Y	154.824	177.415	90.368	90.88	120.448	97.611
	P	—	-195.752	1.497	1.224	1.082	12.198

methods that adjust the response coefficients k of the sensors. The mean value filter algorithm reduces the stripe noise by a constant convolution kernel and convolution neural network. Ours are based on learning, especially as our method is also an adaptive algorithm.

The measurements are in table3 and table4. According to table3, table4, figure8, and figure9, the histogram specification algorithm is of little use for variable stripe noise of AGRI of FY-4A. BP neural network can reduce the stripe noise, but the effect is not good enough to reduce all the noise. Mean value filter is a low-pass filter, which reduces the high-frequency noise in all the directions, so it can reduce the stripe noise, but the image blurs. In all the methods, algorithms based on learning greatly show their effectiveness. The WSVODP of CNN and our method both become smaller and the processed images demonstrate they are useful in

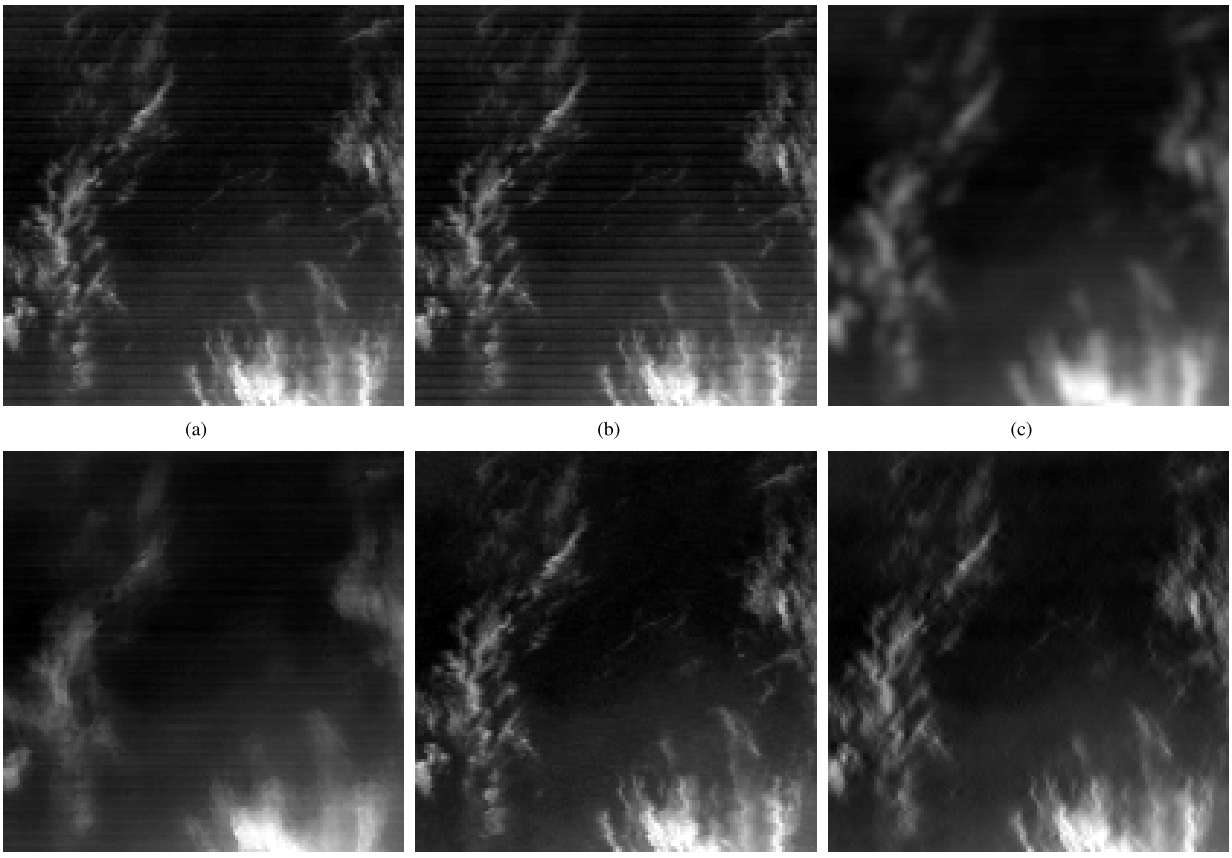

FIGURE 10. Earth surface images processed by (a) Original image (b) Histogram adjusting (c) Mean Value filtering (d) BP neural network (e) Convolution neural network (f) Ours.

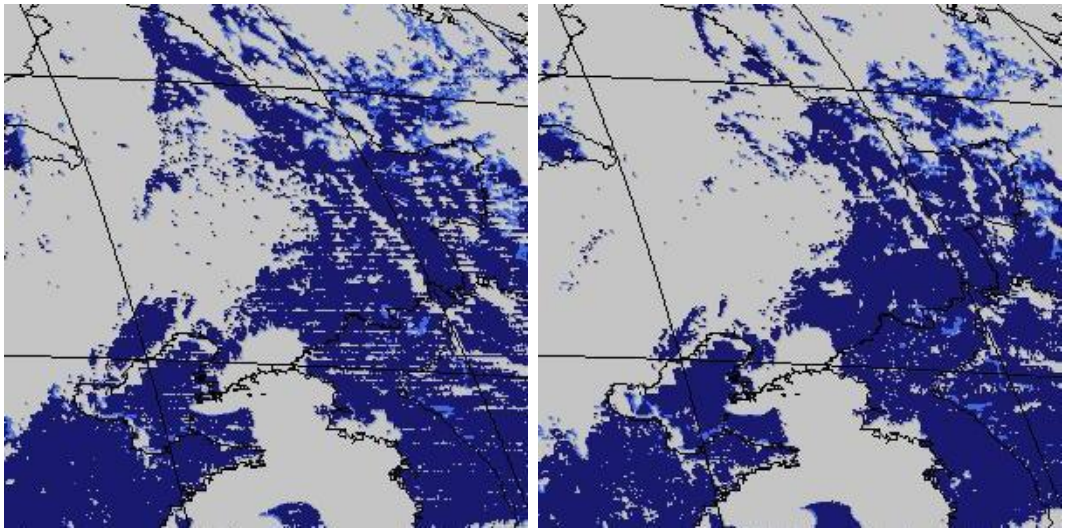

FIGURE 11. Cloud detection (a) Using original image (b) Using processed image.

reducing stripe noise. However, the CNN algorithm needs the characteristics of the images being trained, so the effect is sometimes is good, and sometimes is not good enough. Our method is not only based on learning, but it is also an adaptive algorithm, so the effect is the most steady. WSVODP is almost the smallest, especially as the process is mostly along the horizontal direction with little, along the vertical direction. This keeps the details of the image.

From the dataset, we chose many images with different views at random and all the denoising results are shown

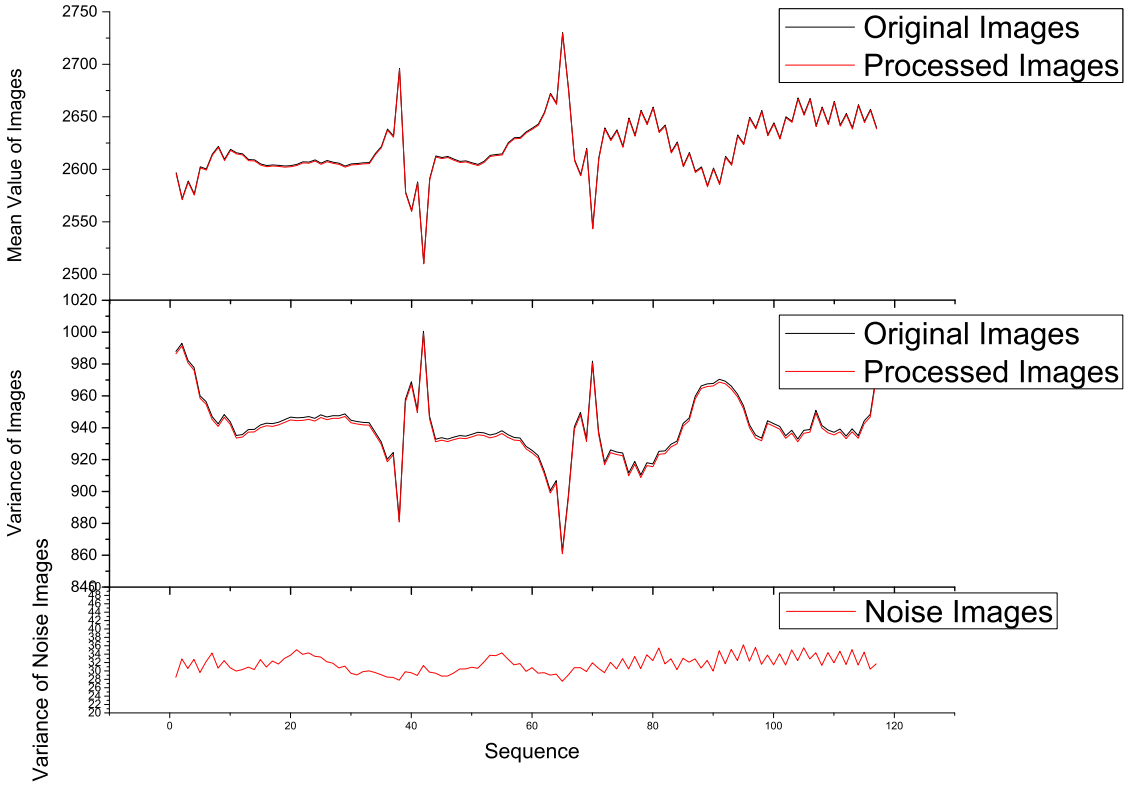

FIGURE 12. Measurements for sequence images.

in appendix A. The result demonstrates that LAWF is very useful in reducing variable stripe noise caused by different SRF of the sensors.

C. APPLICATION

Cloud detection is a fundamental or first step to the applications of remote sensing images and it also plays a curial role in the quantitative applications of FY-4A satellite observation data. The cloud detection algorithm uses the 6.9μm-7.3μm band to detect the middle layer cloud. Two cloud detection images are shown in figure11; figure11a is the cloud detection image at 3AM on Mar. 26 in 2018(UTC), figure11b is the cloud detection image at 4AM on Mar. 26 in 2018(UTC). At this time, the LAWF algorithm began work in the operational system. It is obvious that the cloud detection image using original image is very bad with many incorrect Comb-type clouds appearing in the image, but there are no wrong clouds in the cloud detection image using the denoised image. Therefore, the proposed algorithm is very useful in reducing variable stripe noise.

D. DISCUSSION

Sequence images are processed to monitor the stability of the algorithm. The mean value of the image is the power of the image, the variance of the image is the power distribution of the image, and the variance of the noise image is the power of the noise image. The curves of the three parameters are shown in figure12, the mean value curves before and after processing are nearly the same and the variance curves before and after processing are nearly the same too. This means the image power and the image power distribution hardly vary after reducing the stripe noise. In another words, the wavelet filter only reduces the digital number of high-power lines and raises the digital number of low-power lines, but does not change the total power.

According to the variance of the noise image, the power of the noise image is very steady, which satisfies the character of the noise. In another words, the LAWF algorithm is very stable.

VI. CONCLUSION

After FY-4A was launched successfully, it was found that obvious east-west stripe noise appears in the 6.9μm-7.3μm images and this is ruinous to many applications such as cloud detection. To confirm the reason of stripe noise in the water vapor image, a new concept called Variance of DN Probability is suggested and analysis based on the VODP curve demonstrates that the reason is the different SRF of the 4 sensors.

For reducing stripe noise, a new learning adaptive wavelet filter based on new measurement parameter WSVODP is proposed. WSVODP is linked to the response of sensors to a specific target. It is only sensitive to the response difference, so it is good at determining the

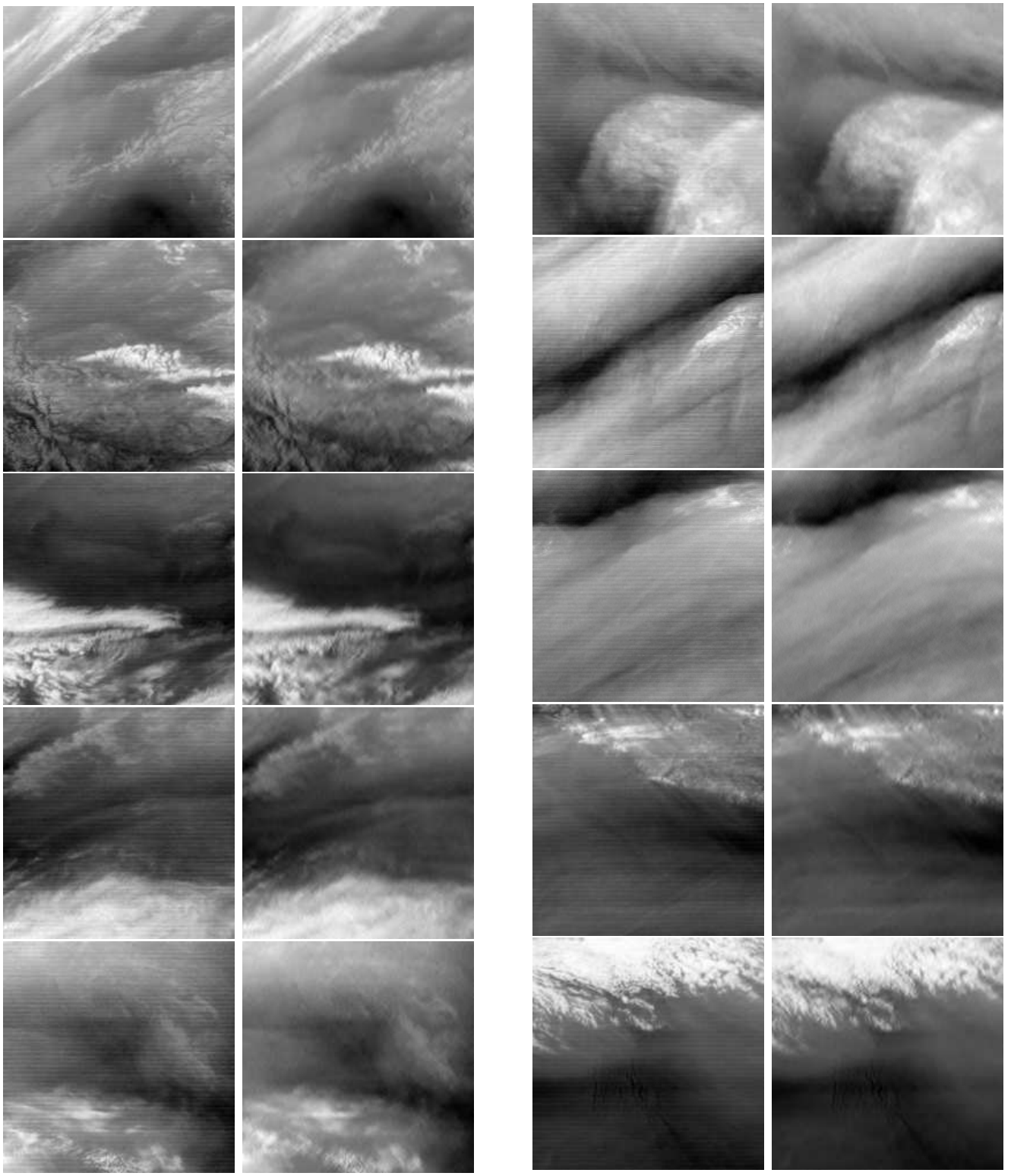

FIGURE 13. Denoising for different views.

filter coefficients. According to the experiment, WSVODP indicates the most appropriate filter coefficients fast and exactly. The measurements of the images and application including cloud detection all prove that the proposed wavelet filter is very good at reducing the variable stripe noise.

At last, a new process is designed based on the scanning model of AGRI in order to avoid ringing artifact. This ensures the high-quality images from the AGRI.

APPENDIX

See figure13.

ACKNOWLEDGMENT

The authors would like to thank the editor and anonymous reviewers for their helpful comments and valuable suggestions.

The suggestions and encourage from Academician Jianmin XU and Professor Caiying WEI are very benefit for the work, the author thanks them very much.

REFERENCES

[1] Q. Chen, Y. Hu, C. Gong, Z. Li, Y. Zhou, and Y. Liu, "Destriping method for mid-infrared image," *J. Remote Sens.*, vol. 16, no. 1, pp. 93–104, Jan. 2012.
[2] C. Ni, Q. Li, and L. Z. Xia, "A novel method of infrared image denoising and edge enhancement," *Signal Process.*, vol. 88, no. 6, pp. 1606–1614, Jun. 2008.
[3] G. J. Kou, Z. S. Wang, and P. Yao, "Filtering methods for different characteristic stripe noise in SAR image," *J. Remote Sens.*, vol. 15, no. 1, pp. 1–12, Jan. 2011.
[4] X. Y. Han and H. J. Zhang, "A method of striping removal noise from the CBERS-02 satellite CCD image," *J. Nanyang Nornal Univ.*, vol. 8, no. 3, pp. 63–65, Mar. 2009.
[5] Y.-Y. Zou, Q. P. Ge, and Y. Han, "Stripe noise of THz image processing based on frequency filtering," *Comput. Eng. Appl.*, vol. 45, no. 17, pp. 241–243, Sep. 2009.
[6] Y. Wang, Q. Chen, D. K. Yin, and B. M. Zhang, "Real-time nonuniformity correction technique for infrared image," *J. Infr. Millim. Waves*, vol. 18, no. 2, pp. 151–155, Apr. 1999.
[7] D. L. Perry and E. L. Dereniak, "Linear theory of nonuniformity correction in infrared staring sensors," *Opt. Eng.*, vol. 32, no. 8, pp. 1854–1859, Aug. 1993.
[8] D. J. Tan and A. Zhang, "Non-uniformity correction based on local histogram specification," *Infr. Technol.*, vol. 35, no. 6, pp. 325–328, Jun. 2013.
[9] H. Shen and L. Zhang, "A MAP-based algorithm for destriping and inpainting of remotely sensed images," *IEEE Trans. Geosci. Remote Sens.*, vol. 47, no. 5, pp. 1492–1502, May 2009.
[10] X. Lu, Y. Wang, and Y. Yuan, "Graph-regularized low-rank representation for destriping of hyperspectral images," *IEEE Trans. Geosci. Remote Sens.*, vol. 57, no. 7, pp. 4009–4018, Jul. 2013.
[11] H. Zhang, W. He, L. Zhang, H. Shen, and Q. Yuan, "Hyperspectral image restoration using low-rank matrix recovery," *IEEE Trans. Geosci. Remote Sens.*, vol. 52, no. 8, pp. 4729–4743, Aug. 2014.
[12] G. Zhou, H. Fang, C. Lu, S. Wang, Z. Zuo, and J. Hu, "Robust destriping of MODIS and hyperspectral data using a hybrid unidirectional total variation model," *Optik*, vol. 126, nos. 7–8, pp. 838–845, Apr. 2015.
[13] W. Zhao, H. Lu, and D. Wang, "Multisensor image fusion and enhancement in spectral total variation domain," *IEEE Trans. Multimedia*, vol. 20, no. 4, pp. 866–879, Apr. 2018.
[14] D. A. Scribner, K. A. Sarkady, M. R. Kruer, J. T. Caulfield, J. D. Hunt, and C. Herman, "Adaptive nonuniformity correction for IR focal-plane arrays using neural networks," *Proc. SPIE*, vol. 1541, pp. 100–109, Nov. 1991.
[15] B. Y. Chen, L. H. Wen and J. H. Yu, "Scene-based non-uniformity correction for infrared imaging scanner," *Infr. Laser Eng.*, vol. 37, pp. 611–614, Jun. 2008.
[16] B. Y. Chen, "Non-uniformity correction based on complex neural network based on fixed scene," *Chin. J. Sens. Actuators*, vol. 29, no. 8, pp. 1217–1221, Aug. 2016.
[17] S. Ge, S. Zhao, C. Li, and J. Li, "Low-Resolution face recognition in the wild via selective knowledge distillation," *IEEE Trans. Image Process.*, vol. 28, no. 4, pp. 2051–2062, Apr. 2019.
[18] J. Guan, R. Lai, and A. Xiong, "Wavelet deep neural network for stripe noise removal," *IEEE Access*, vol. 7, pp. 44544–44554, 2019. doi: 10.1109/ACCESS.2019.2908720.
[19] H. Lu, Y. Li, T. Uemura, H. Kim, and S. Serikawa, "Low illumination underwater light field images reconstruction using deep convolutional neural networks," *Future Gener. Comput. Syst.*, vol. 82, pp. 142–148, May 2018.
[20] D. L. Donoho, "De-noising by soft-thresholding," *IEEE Trans. Inf. Theory*, vol. 41, no. 3, pp. 613–627, May 1995.
[21] X. Jin, Y. Li, N. Liu, X. Li, Q. Zhou, Y. Tian, and S. Ge, "Scene relighting using a single reference image through material constrained layer decomposition," in *Proc. Int. Symp. Artif. Intell. Robot. (ISAIR)*, Kitakyushu, Japan, Nov. 2017, pp. 25–26.
[22] X. Chen, H. Wu, X. Jin, and Q. Zhao, "Face illumination manipulation using a single reference image by adaptive layer decomposition," *IEEE Trans. Image Process.*, vol. 22, no. 11, pp. 4249–4259, Nov. 2013.
[23] R. Lan, H. Lu, Z. Liu, and X. Luo, "An LBP encoding scheme jointly using quaternionic representation and angular information," *Neural Comput. Appl.*, vol. 31, pp. 1–7, Jan. 2019. doi: 10.1007/s00521-018-03968-y.
[24] G. Liu and X. Shao, "An improved denoising method of structured light image based on wavelet transform," in *Proc. Int. Conf. Adv. Mater., Machinery, Elect. Eng.*, 2017. doi: 10.2991/ammee-17.2017.55.
[25] L. Zhang, L. Zhang, and L. Zhang, "Application research of digital media image processing technology based on wavelet transform," *EURASIP J. Image Video Process.*, vol. 2018, p. 138, Dec. 2018.
[26] S. Huang, Z. Liu, Y. Wang, and R. Wang, "Wide-stripe noise removal method of hyperspectral image based on fusion of wavelet transform and local interpolation," *Opt. Rev.*, vol. 24, no. 2, pp. 177–187, Apr. 2017.
[27] X. Zhang and S. L. Tang, "Destriping remote sensing imagery by wavelet moment matching algorithm," *Remote Sens. Technol. Appl.*, vol. 33, no. 2, pp. 305–312, Apr. 2018.
[28] M. Zhao, B. An, and C. Lin, "Stripe nonuniformity correction algorithm based on steering kernel fitting for single infrared images," *Infr. Laser Eng.*, vol. 43, no. 3, pp. 764–771, Mar. 2014.
[29] S. Zhang, W. Xiang, and Y. Zhan, "Stripe noise removal method for infrared images based on guided filtering," *J. Comput.-Aided Des. Comput. Graph.*, vol. 29, no. 8, pp. 1434–1443, Aug. 2017.
[30] X. Jin, Y. Li, N. Liu, X. Li, X. Jiang, C. Xiao, and S. Ge, "Single reference image based scene relighting via material guided filtering," *Opt. Laser Technol.*, vol. 110, pp. 7–12, Feb. 2019.
[31] S. P. Wang and T. Gao, "Destriping method for infrared image based on bilateral filter," *Infr. Technol.*, vol. 36, no. 9, pp. 728–731, Sep. 2014.
[32] X. Chen, M. Chen, X. Jin, and Q. Zhao, "Face illumination transfer through edge-preserving filters," in *Proc. IEEE Int. Conf. Comput. Vis. Pattern Recognit. (CVPR)*, Colorado Springs, CO, USA, Jun. 2011, pp. 281–287.

BOYANG CHEN was born in Haerbin, Heilongjiang, China, in 1980. He received the B.S. degree from the University of Science and Technology of China (USTC), in 2003, and the Ph.D. degree from the Chinese Academy of Sciences, in 2008.

He is currently a Faculty Member with the National Satellite Meteorological Center, Beijing, China. His research interests include calibration and validation, image processing, and image assessment. He is also the Leader of calibration and validation system of ground segment of FY-4A, and many new preprocess technologies for FY-4A have been done, including calibration and radiance validation, spectrum calibration, on-orbit MTF measurement, and image enhance.

XUAN FENG received the Ph.D. degree from the Anhui Institute of Optics and Fine Mechanics, Chinese Academy of Sciences, Anhui, China, in 2007. She is currently an Associate Researcher with the Technology and Engineering Center for Space Utilization, Chinese Academy of Sciences, Beijing, China. Her research interests include on-orbit radiometric calibration, spectral calibration, and specification evaluation for spaceborne instruments.

RONGHUA WU received the B.S. degree in physics from Beijing Normal University, Beijing, China, in 2005, and the M.S. degree from the Chinese Academy of Meteorological Sciences, Beijing, China, in 2010. He is currently a Senior Engineer with the National Satellite Meteorological Center, China Meteorological Administration, Beijing, with a focus on FY-3 data preprocessing, including geo-location and radiation calibration.

QIANG GUO received the M.S. degree in signal and information processing and the Ph.D. degree in electronic science and technology, with a focus on specifications, including spatial resolution and detection sensitivity, and on-orbit evaluation for spaceborne remotely sensed instrument, from the Shanghai Institute of Technical Physics, Chinese Academy of Sciences, Shanghai, China, in 2001 and 2003, respectively.

He is currently the second Chief Designer of the ground-segment systems for both Fengyun-2 and Fengyun-4 serial satellites. His research interests include on-orbit radiometric calibration, geolocation, and specification evaluation for spaceborne instruments.

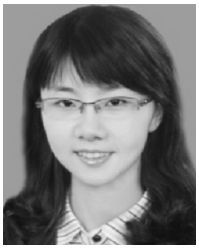

XI WANG received the Ph.D. degree in atmospheric physics and environment from Peking University, Beijing, China, in 2013. Since then, she has been with the National Satellite Meteorological Center, China Meteorological Administration. She is currently working on remote sensing of clouds, cloud mask, and related analysis.

SHIMING GE (M'13–SM'15) received the B.S. and Ph.D. degrees in electronic engineering from the University of Science and Technology of China (USTC), in 2003 and 2008, respectively. He was a Senior Researcher with Shanda Innovations and a Researcher with Samsung Electronics and the Nokia Research Center. He is currently an Associate Professor with Institute of Information Engineering, Chinese Academy of Sciences. His research interests include computer vision, deep learning, and AI security, especially efficient and secure deep learning models toward scalable applications.